Supporting Information

Multifunctional CuO/Cu_2O Truncated Nanocubes as Trimodal Image-Guided Near Infrared-III Photothermal Agents to Combat Multidrug Resistant Lung Carcinoma

*Munusamy Shanmugam[1], Naresh Kuthala[1†], Raviraj Vankayala[2†], Chi-Shiun Chiang[3], Xiangyi Kong[4], Kuo Chu Hwang[1]**

[1]Department of Chemistry, National Tsing Hua University, Hsinchu 30013, Taiwan ROC

[2]Department of Bioscience and Bioengineering, Indian Institute of Technology Jodhpur, Karwar 342037, Jodhpur, Rajasthan, India

[3]Department of Biomedical Engineering and Environmental Sciences, National Tsing Hua University, Hsinchu 30013, Taiwan ROC

[4]Department of Breast Surgical Oncology, National Cancer Center/National Clinical Research Center for Cancer/Cancer Hospital; Chinese Academy of Medical Sciences and Peking Union Medical College, Beijing, 100021, China

†Equally contributed.

*E-mail: kchwang@mx.nthu.edu.tw

Methods

Photothermal conversion efficiencies:

Photothermal conversion efficiency PCE (η) was determined for CuO/Cu_2O NCs by irradiating light intensities of 808, 1064 and 1550 nm (300 mW/cm^2) for 9 min to reach the steady state temperature. Then, the laser was turned off and the temperature was recorded. The values of PCE (η) was calculated based on the following equations as reported in the literature.[S1]

$$\eta = [hS (T_{max} - T_{surr}) - Q_{dis}] / I (1\text{-}10^{-A_{808}}) \quad \ldots\ldots\ldots\ldots\ldots (1)$$

The heat absorbed Q_{dis} was calculated to be 14.34 mW, I is the laser power intensity (300 mW/cm^2) and the absorbance of CuO/Cu_2O NCs is 0.5. Where h is the coefficient of heat transfer; S is the surface area; T_{max} is the maximum temperature; and T_{surr} refers to the surrounding temperature, respectively. The value of hS was estimated using following expression

$$hS = mD \times cD / \zeta s \quad \ldots\ldots\ldots\ldots\ldots\ldots\ldots\ldots\ldots\ldots\ldots\ldots\ldots\ldots\ldots (2)$$

Heat dissipation time constant (ζs) was determined by plotting the linear data of cooling period with the negative natural logarithm as expressed below

$$t = - \zeta s \ln(\theta) \quad \ldots\ldots\ldots\ldots\ldots\ldots\ldots\ldots\ldots\ldots\ldots\ldots\ldots\ldots\ldots\ldots\ldots\ldots\ldots\ldots (3)$$

$$\theta = [T - T_{surr}]/ [T_{max} - T_{surr}] \ldots\ldots\ldots\ldots\ldots\ldots\ldots\ldots\ldots\ldots\ldots\ldots (4)$$

Therefore, hS = 0.35*4.2/213.317 J/sec ^{o}C = 6.89 mW/ ^{o}C

$$\eta_{808\ nm} = 6.89*(23.7) -14.34/ 300 (1-10^{\wedge-0.5})$$

$$= 72.62\%$$

The photothermal efficiencies for 1064 and 1550 nm were estimated, respectively, in a similar fashion. The heat absorbed Q_{dis} were calculated as 13.12 and 15.56 mW, respectively, while the values of laser power intensity (300 mW/cm^2) and absorbance (A= 0.5) of CuO/Cu_2O NCs are same.

$$\eta_{1064\ nm} = 9.06*(16.6)-13.12/300 (1-10^{\wedge-0.5})$$

$$= 67\%$$

$$\eta_{1550\ nm} = 7.17*(24.4)- 15.56/ 300 (1-10^{\wedge-0.5})$$

$$= 77.7\%$$

Singlet O_2 phosphorescence quantum yield:

The quantum yield for generation of singlet O_2 phosphorescence by CuO/Cu_2O TNCs upon 1064 nm light excitation was calculated by using methylene blue (MB) as a reference standard. Phosphorescence emission area, $Area_{phos,MB}$ is the multiplication product of absorbance of methylene blue at 650 nm (Ab_{MB-650}), incident light intensity at 650 nm (2 mW/cm^2, slit width: 10 nm) from the luminescence spectrometer, and the singlet O_2 formation yield (Φ_{MB}), *i.e.*, the equation (5). The singlet O_2 quantum yield of MB in D_2O is known to be 0.68.[S2]

$$Area_{phos\text{-}MB} = Ab_{MB\text{-}650} \times I_{650} \times \Phi_{MB} \ldots\ldots\ldots\ldots\ldots (5)$$

$$Area_{phos\text{-}MB} = 282312$$

Similar equation can be derived for plasmonic CuO/Cu_2O TNCs (see equation (6))

$$Area_{phos\text{-}CuO/Cu2O\text{-}1064\ nm} = Ab_{phos\text{-}CuO/Cu2O\text{-}1064\ nm} \times I_{1064} \times \Phi_{CuO/Cu2O\text{-}1064\ nm} \ldots\ldots\ldots (6)$$

$$Area_{phos\text{-}\ CuO/Cu2O\text{-}1064\ nm} = 662584$$

The phosphorescence emission area under the curve can be obtained by integrating the area between 1225 to 1300 nm. The absorbance value was determined to be 0.8 for plasmonic CuO/Cu_2O TNCs from the UV-visible NIR spectrometer. From the photoluminescence spectrometer (FLS920) at a slit width of 10 nm, the light intensity is 8.3 mW/cm^2 at 1064 nm. Upon substituting all the parameters and dividing equations (5)/(6) the value of $\Phi_{CuO/Cu2O\ TNCs\text{-}1064\ nm}$ obtained is 0.24.

Measurement of fluorescence quantum yield of plasmonic CuO/Cu_2O Truncated Nanocubes.

Fluorescence quantum yield of plasmonic CuO/Cu_2O Truncated Nanocubes upon 1064 nm excitation was determined using standard dye IR 125 as a reference. The fluorescence quantum yield (Φ_f) for plasmonic CuO/Cu_2O TNCs at 1064 nm can be calculated based on the equation as reported in the literature. [S3]

$$\Phi_{f\,TNCs} = \Phi_{f\,IR\text{-}125} \times (I_{TNCs}/I_{IR\text{-}125}) \times (OD_{IR\text{-}125}/OD_{TNCs}) \times (n_{TNCs}/n_{IR\text{-}125})^2 \ldots\ldots\ldots\ldots (7)$$

$\Phi_{f\,TNCs}$ and $\Phi_{f\,IR\text{-}125}$ are the fluorescence quantum yields of plasmonic CuO/Cu_2O TNCs and IR-125, respectively. I_{TNCs} and $I_{IR\text{-}125}$ are the integrated fluorescence area obtained by integrating area from (1200-1600 nm) for CuO/Cu_2O TNCs and (750-1000 nm) for IR-125, respectively. $OD_{IR\text{-}125}$ and OD_{TNCs} are the optical density values for the dye and CuO/Cu_2O TNCs, respectively. n_{TNCs} and $n_{IR\text{-}125}$ are the corresponding refractive indices of the solvent used for dissolving CuO/Cu_2O TNCs and IR-125, respectively. Here, water was used as a solvent to dissolve CuO/Cu_2O TNCs and DMSO to dissolve IR-125 and their specific refractive index values are known to be 1.33 and 1.47, respectively. [S3] The fluorescence quantum yield of IR-125 in DMSO is known to be 0.132. [S3]

$$\Phi_{f\,TNCs} = 0.132 \times 370369/532463 \times (1.33/1.47)^2$$

$$= 0.074$$

Upon substituting all the parameters in equation (7) one can obtain the value of $\Phi_{f\,TNCs}$ to be 0.074 for 1064 nm excitation.

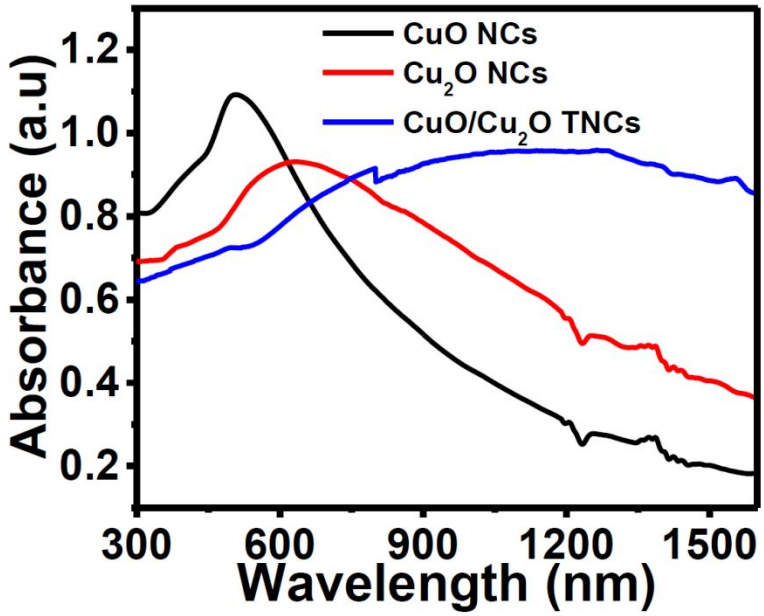

Figure S1. UV-Vis-NIR spectra of CuO NCs, Cu_2O NCs and plasmonic CuO/Cu_2O TNCs, respectively.

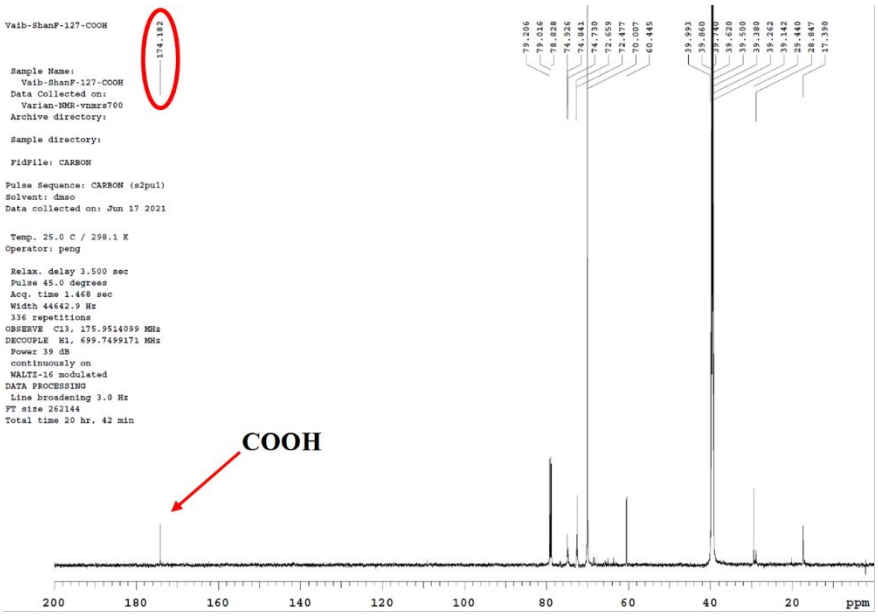

Figure S2. ^{13}C-NMR spectrum of pluronic F127-COOH polymer.

.

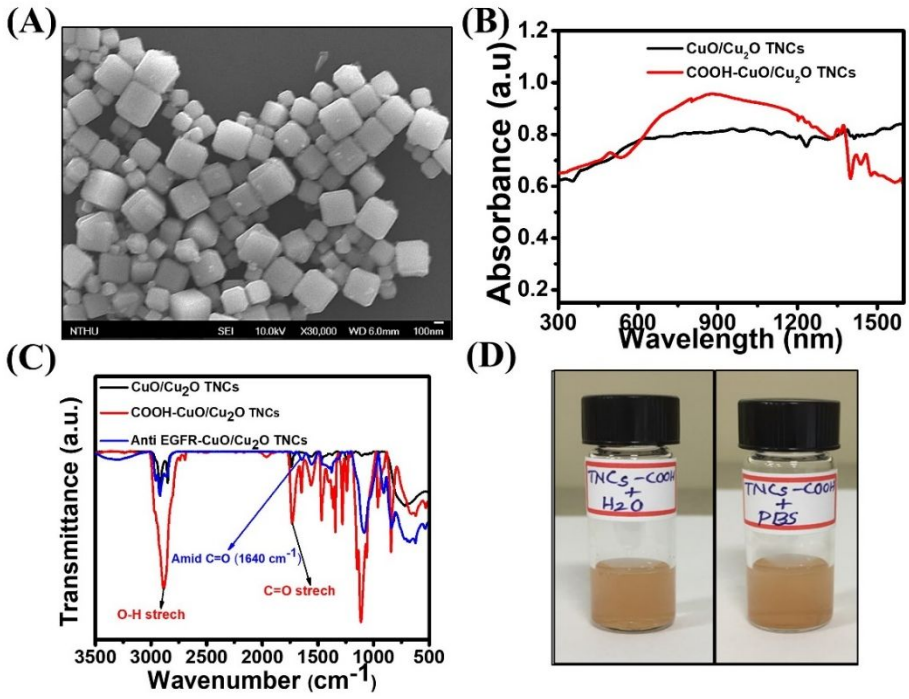

Figure S3. (A) SEM image for F127-COOH conjugated plasmonic CuO/Cu_2O TNCs. (B) UV-vis-NIR absorption spectra of plasmonic CuO/Cu_2O TNCs before and after conjugation of F127COOH. (C) FTIR spectra for plasmonic CuO/Cu_2O TNCs, COOH-CuO/Cu_2O TNCs and anti EGFR-CuO/Cu_2O TNCs, respectively. (D) Dispersion stabilities of F127-COOH conjugated CuO/Cu_2O TNCs in water and PBS, respectively.

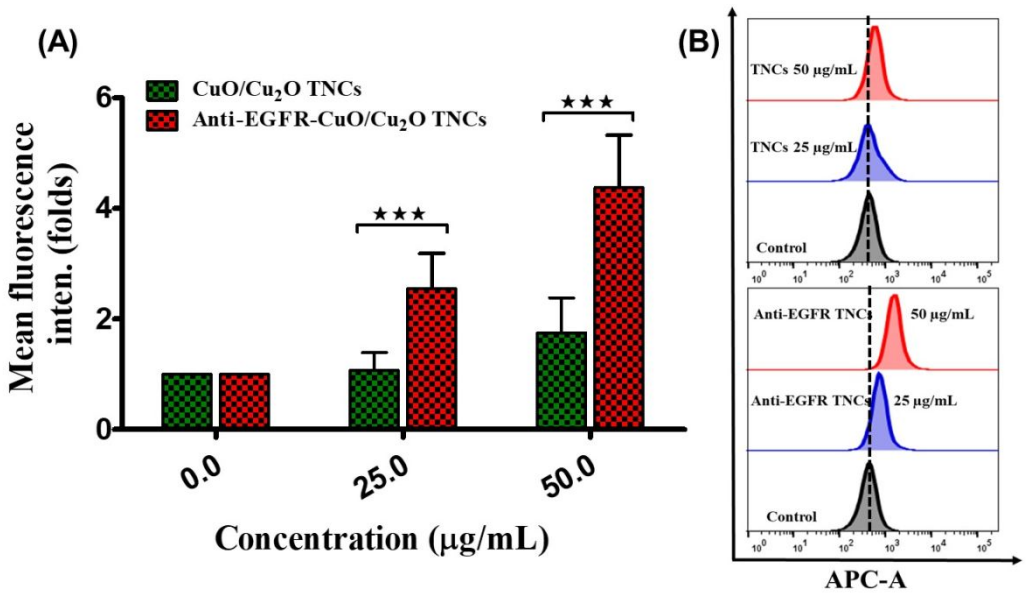

Figure S4. *In vitro* cellular uptake of CuO/Cu_2O TNCs (without anti EGFR on the surface), and anti EGFR-CuO/Cu_2O TNCs-internalized H69AR cells monitored using flow cytometry.

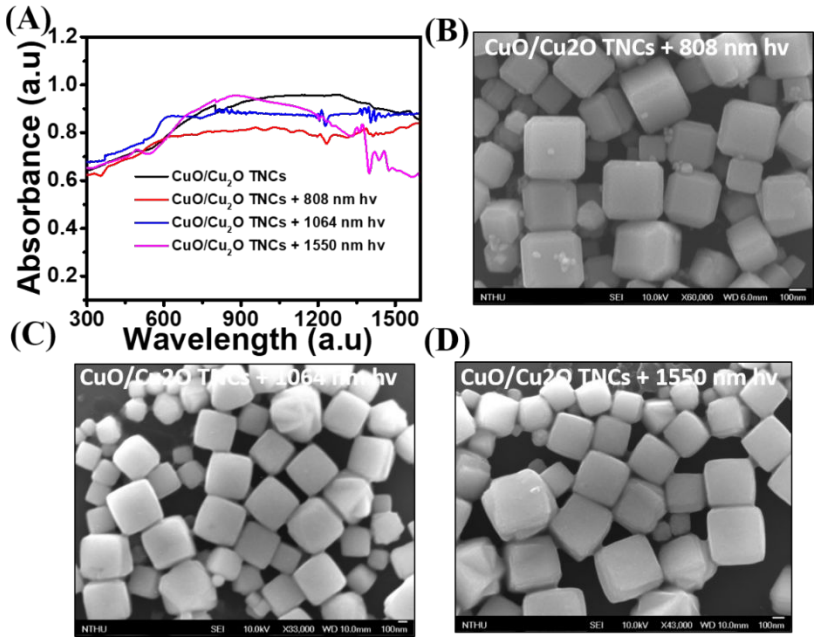

Figure S5. Photostability of plasmonic CuO/Cu_2O TNCs upon light illumination using 808 nm, 1064 nm and 1550 nm CW lasers, respectively.

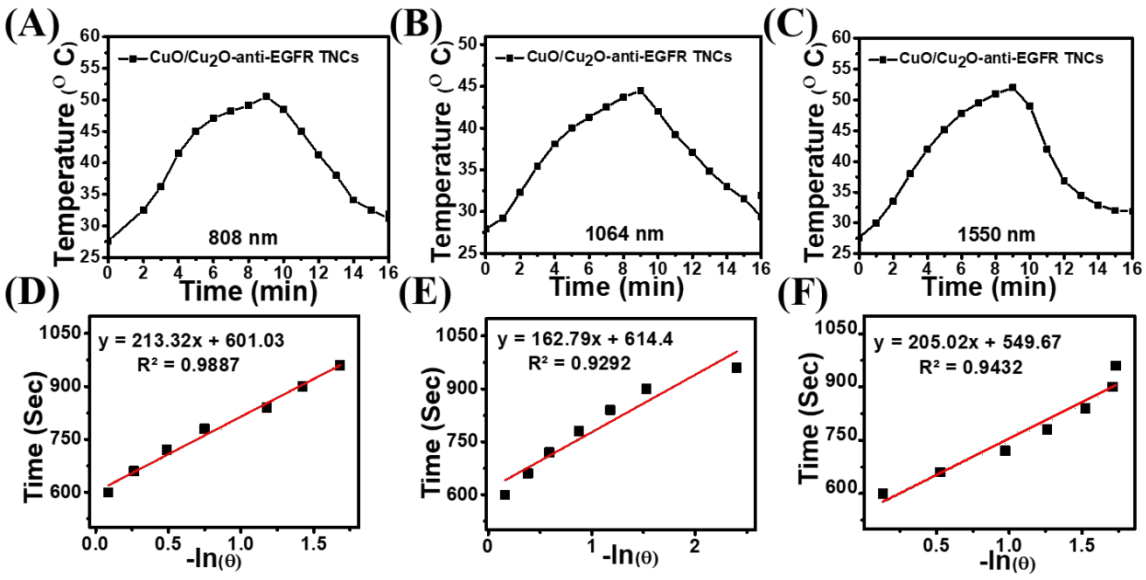

Figure S6. Photothermal conversion abilities of CuO/Cu_2O TNCs on laser irradiation at (A) 808, (B) 1064 and (C) 1550 nm, respectively.

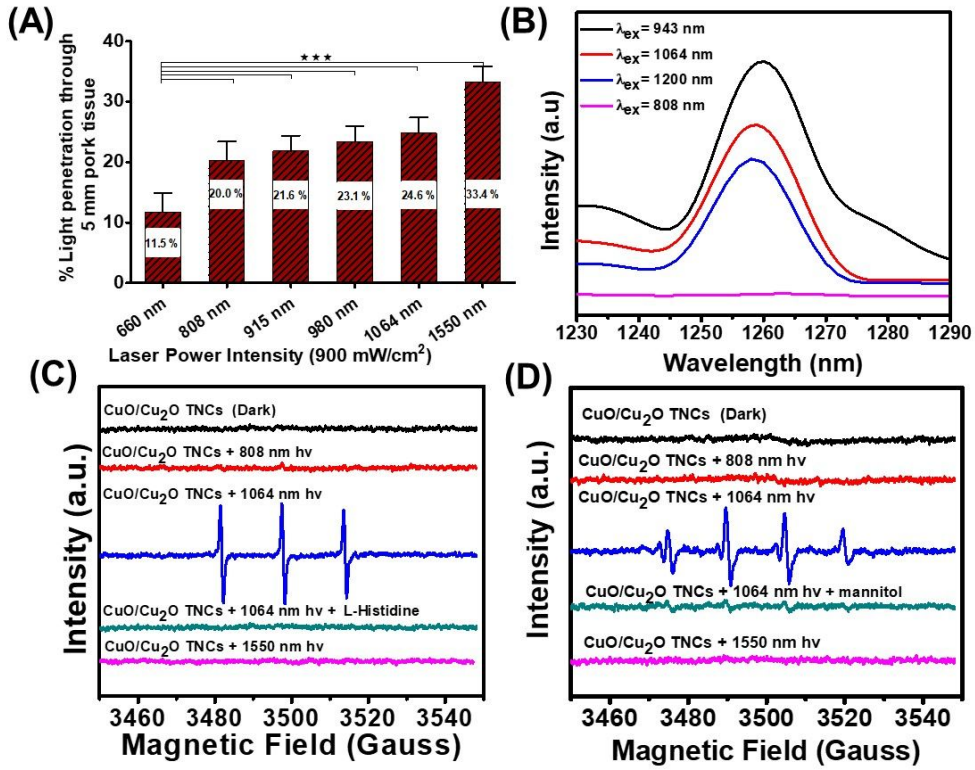

Figure S7. *Photodynamic and photothermal capabilities of* anti EGFR-*CuO/Cu$_2$O TNCs*. (A) The percentages of light penetration through a pork tissue of ~ 5 mm thickness for different lasers (660, 808, 915, 980, 1064 and 1550 nm) at a power intensity of 900 mW/cm^2 (Note that the percentages of light penetration were meaured at the time point after 9 min continuous irradiation of a given wavelength. After 9 min irradiation, the detected light intensity through the pork tissue becomes more stable with little fractuation). (B) Singlet oxygen phosphorescence emission spectra at 808, 943, 1064, and 1200 nm excitation wavelengths, respectively. (C) and (D) EPR spectra of $^1O_2$ and OH radical CuO/Cu$_2$O TNCs, respectively. The statistically significant differences are indicated as $*p < 0.05$, $**p < 0.01$, and $***p < 0.001$.

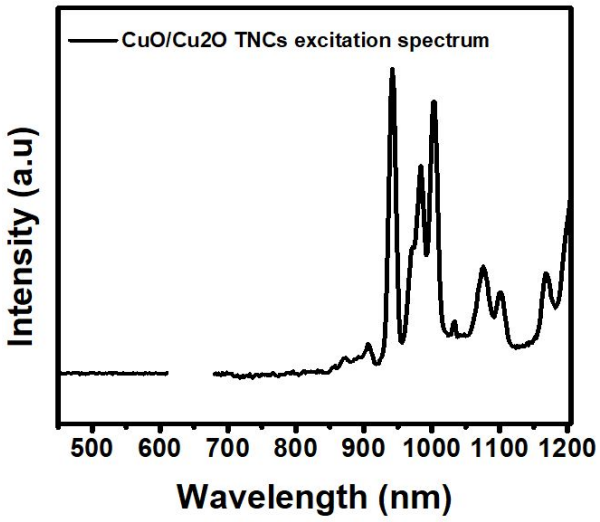

Figure S8. Excitation spectrum for singlet oxygen phosphorescence emission of anti EGFR-CuO/Cu_2O TNCs ((the emission wavelength was set at λ_{em} = 1260 nm).

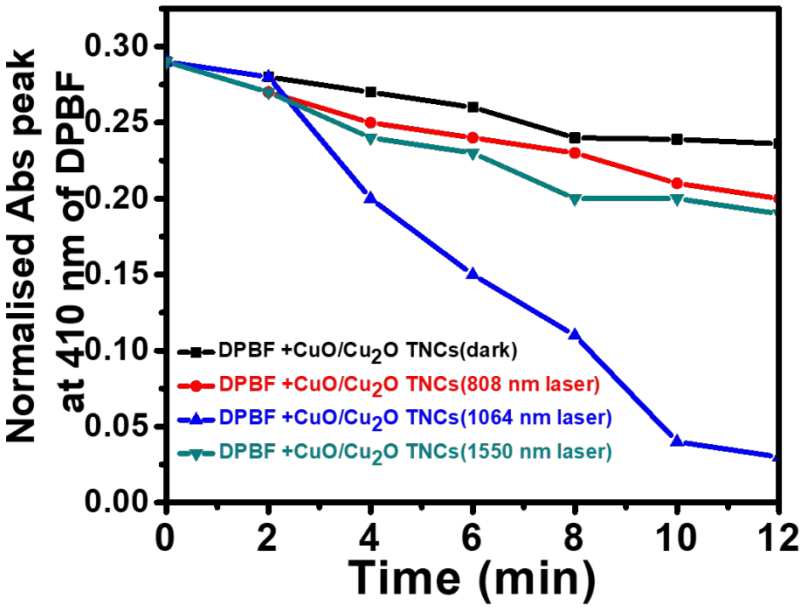

Figure S9. Singlet oxygen generation monitoring by using DPBF solution incubated with CuO/Cu_2O TNCs under (a) dark, (b) 808 nm, (c) 1064 nm, and (d) 1550 nm laser irradiation, respectively (power densities for all wavelengths are the same, 300 mW/cm^2).

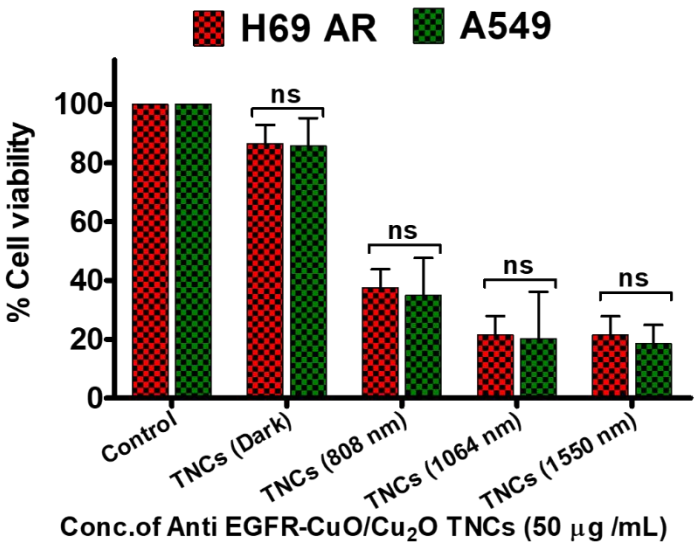

Figure S10. Cellular viabilities of anti-EGFR-CuO/Cu_2O TNCs (50 μg/mL)-internalized H69AR and A549 cells under dark and various photo-irradiation conditions.

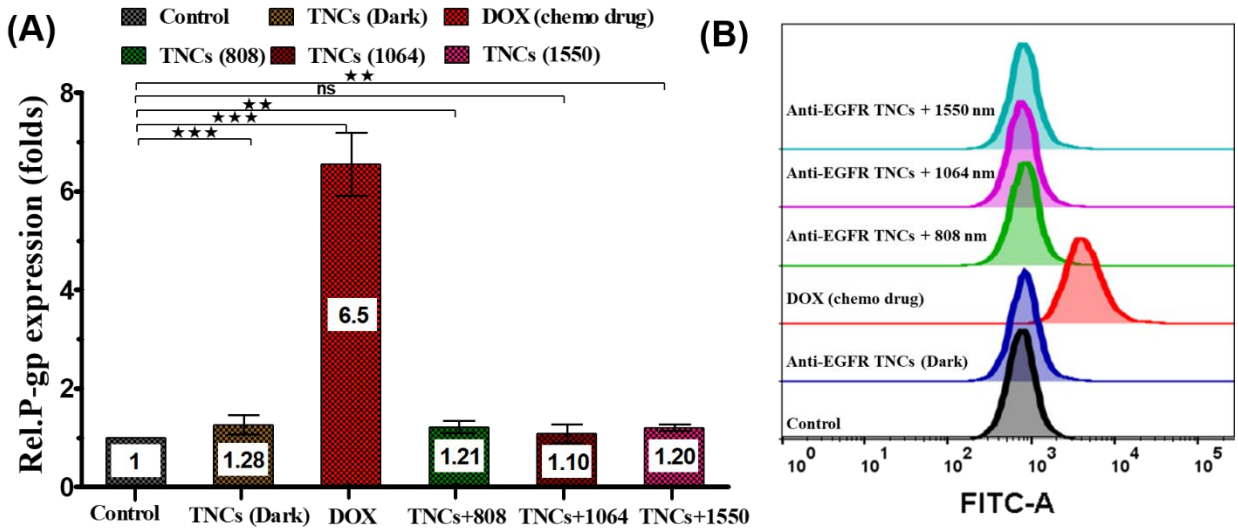

Figure S11. P-glycoprotein expression levels of DOX, anti-EGFR-CuO/Cu_2O TNCs and CuO/Cu_2O TNCs-internalized H69AR cells under dark and various photo-irradiation conditions. *$p < 0.05$, **$p < 0.01$, ***$p < 0.001$.

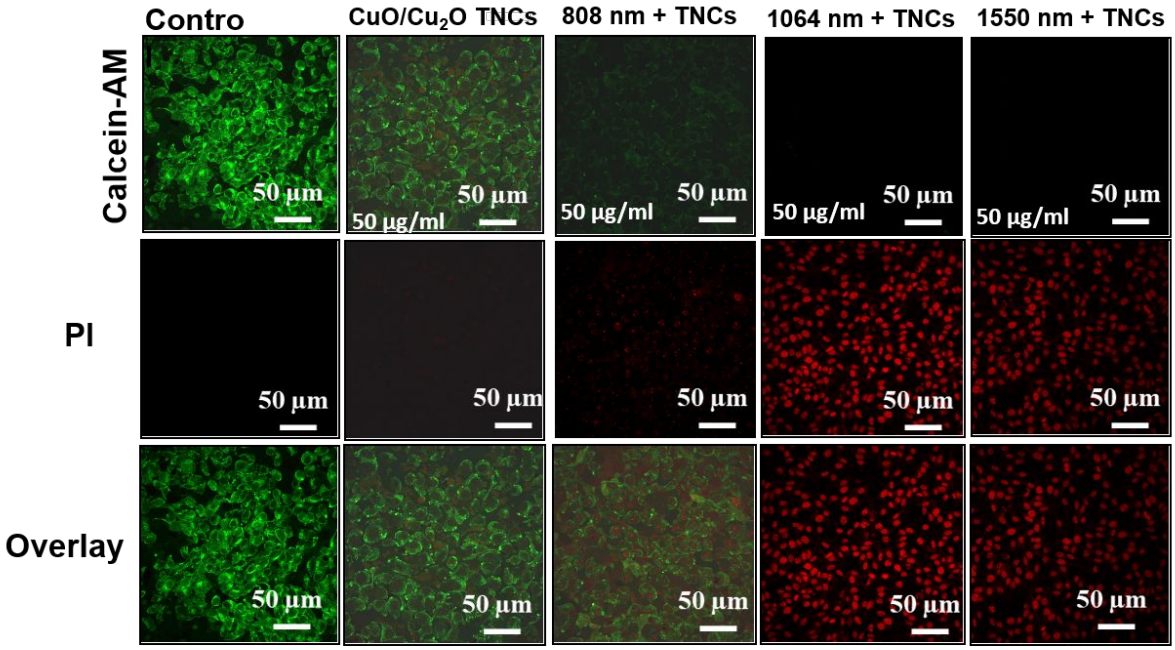

Figure S12. LIVE/DEAD assay of the Anti EGFR-CuO/Cu_2O TNCs internalized H69AR cells under dark and photo-irradiation conditions. The live cells were stained with calcein AM (false colored in green), and the dead cells were stained with PI (false colored in red), respectively. Scale bar represents 50 µm.

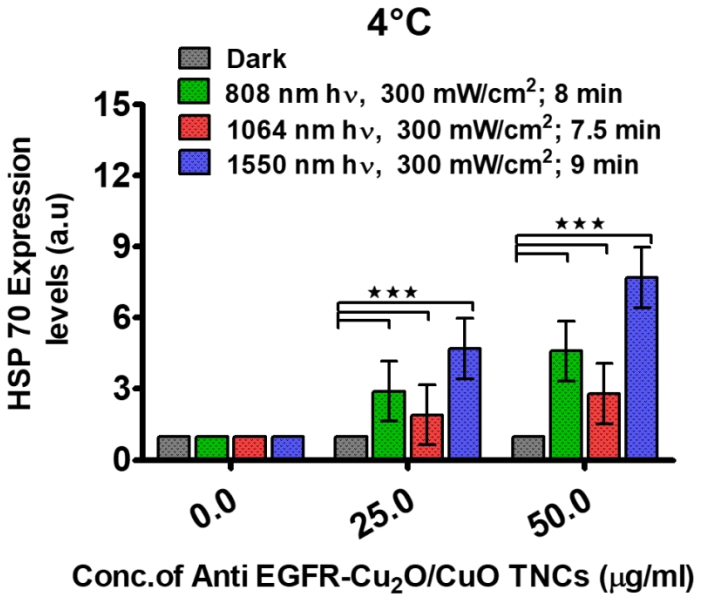

Figure S13. Photo-induced expression of HSP 70 levels for anti EGFR-CuO/Cu_2O TNCs internalized H69 AR cells at 4°C incubation. $*p < 0.05$, $**p < 0.01$, $***p < 0.001$.

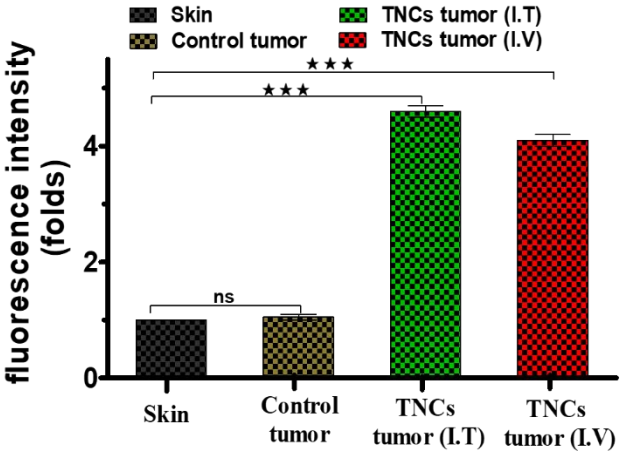

Figure S14. Quantification of NIR fluorescence intensities near the tumor regions for the mice injected with PBS (control group), intratumoral (IT) and intravenous (IV) injection of anti EGFR-CuO/Cu_2O TNCs, respectively (n=3). The statistically significant differences are indicated as $*p < 0.05$, $**p < 0.01$, and $***p < 0.001$.

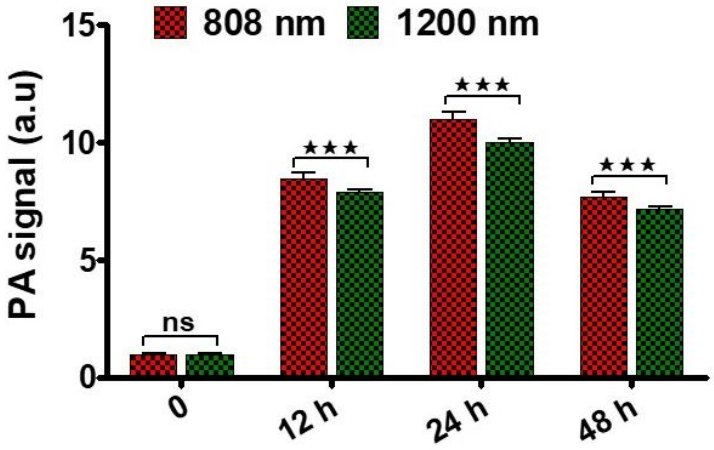

Figure S15. Photoacoustic signal intensities of anti EGFR-CuO/Cu_2O TNCs at 0, 12, 24 and 48 h post intravenous injection using 808 nm (NIR I BW) and 1200 nm (NIR II BW) light excitation, respectively. The statistically significant differences are indicated as $*p < 0.05$, $**p < 0.01$, and $***p < 0.001$.

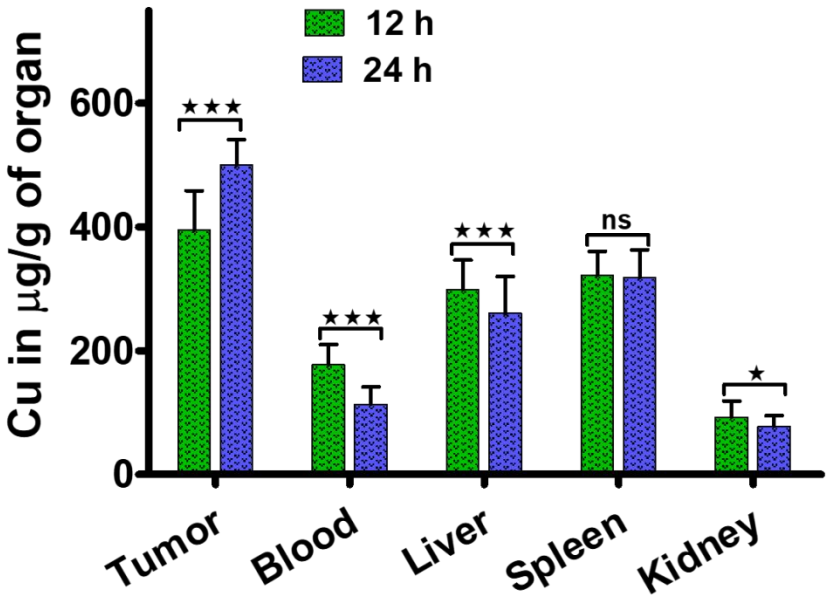

Figure S16. *In vivo* biodistribution of anti EGFR-CuO/Cu_2O TNCs in H69AR tumor bearing mice using ICP-MS analysis. ∗p < 0.05, ∗∗p < 0.01, ∗∗∗p < 0.001.

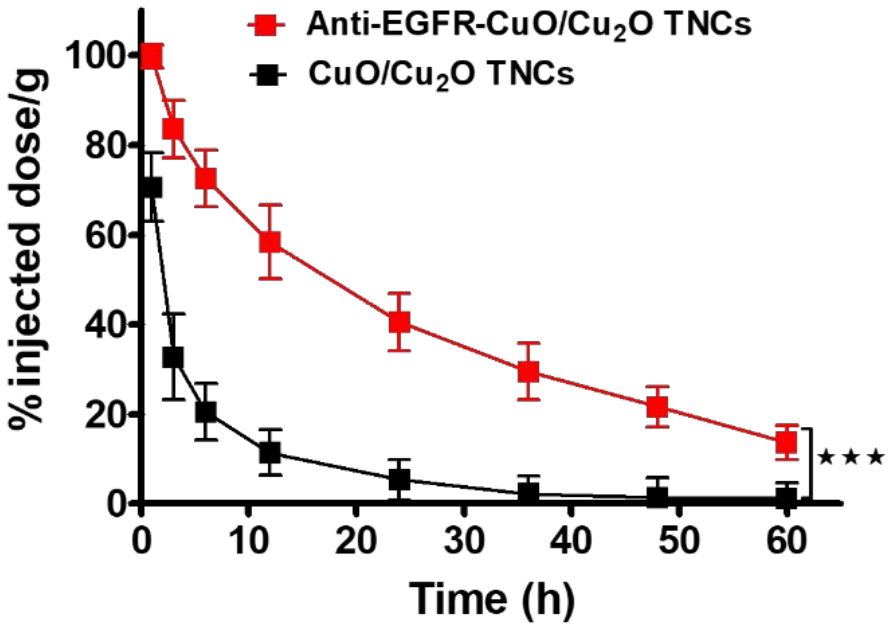

Figure S17. *In vivo* pharmacokinetic studies of anti EGFR-CuO/Cu_2O TNCs and CuO/Cu_2O TNCs (without anti EGFR on the surface) in healthy mice at various time points 1, 3, 6, 12, 24, 36, 48 and 60 h after iv injection of nanoparticles, respectively. The statistically significant differences are indicated as ∗p < 0.05, ∗∗p < 0.01, and ∗∗∗p < 0.001.

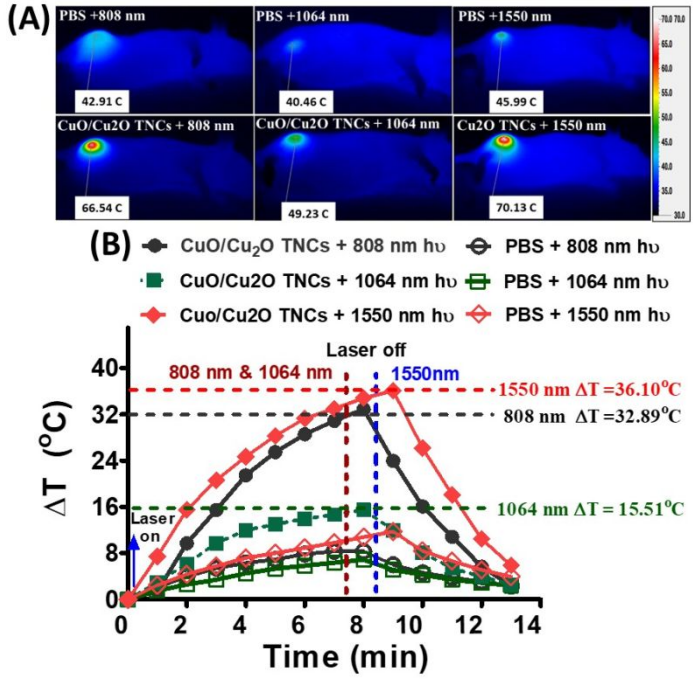

Figure S18. (A*) In vivo* photothermal images of mice under different conditions as labeled in the figure. The values indicated are the final temperatures for the mice exposed to different laser wavelengths. (B) The change in temperature rise profiles were plotted as a function of the irradiation time for different conditions.

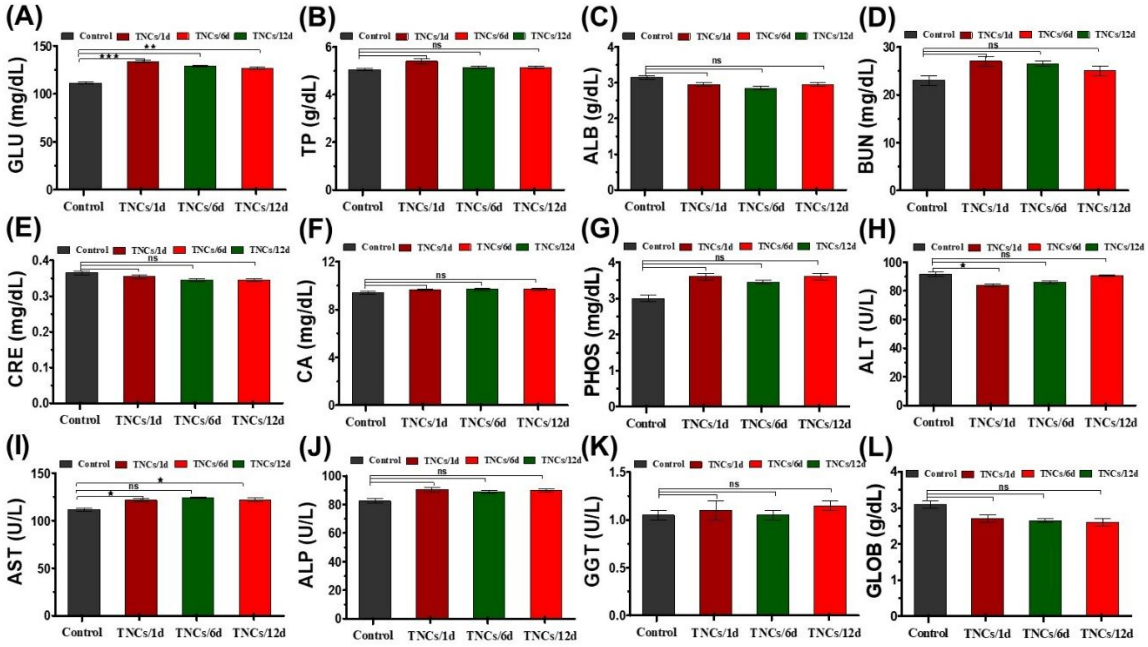

Figure S19. *In vivo* blood biochemistry evaluation of anti-EGFR-CuO/Cu_2O TNCs (50 mg/kg) in healthy mice at 1, 6 and 12 day post intravenous injection. The control mice were injected with PBS and the toxicity values were performed at day 12 as the control value for comparison.

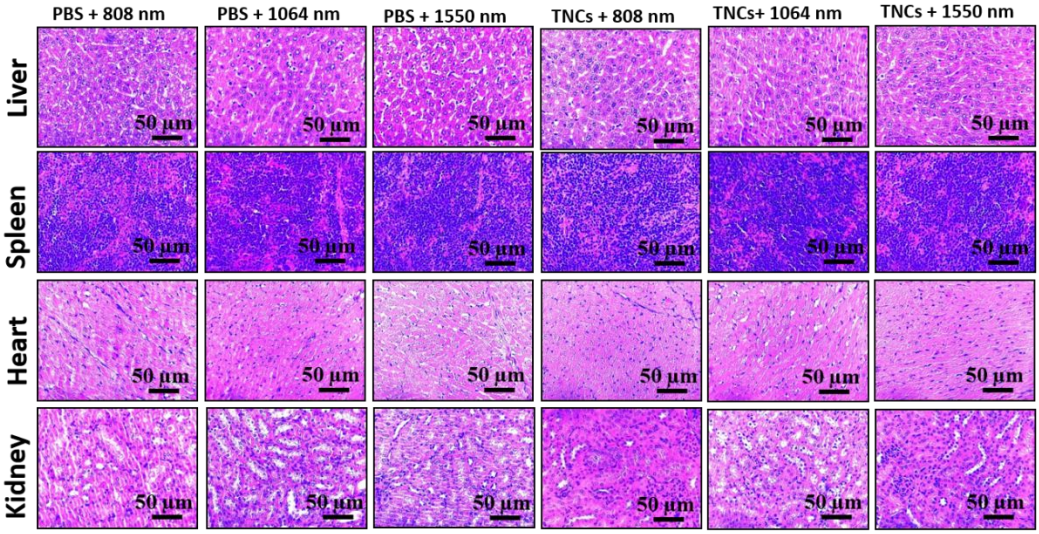

Figure S20. H&E staining images of liver, spleen, heart and kidney sections of anti EGFR-CuO/Cu_2O TNCs in H69 AR tumor bearing mice under 808 nm, 1064 nm and 1550 nm photoirradiation conditions, respectively. The scale bar indicates 50 µm.

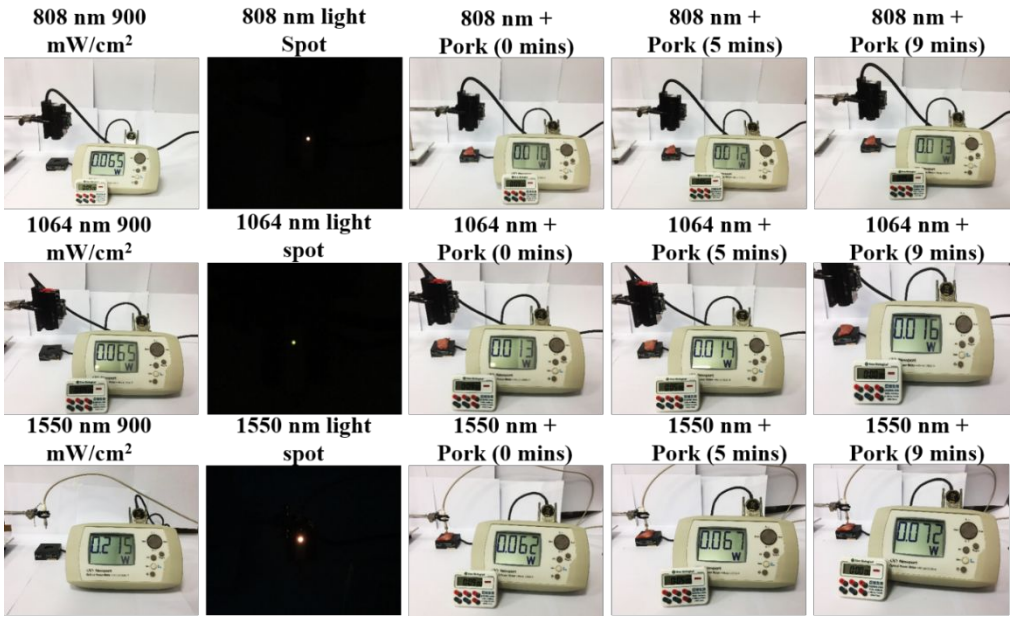

Figure S21. Optical images showing the experimental setup of light penetration through a pork tissue of 0.5 cm thickness for different laser wavelengths (808, 1064 and 1550 nm; all have the same laser power intensities of 900 mW/cm²). The pork tissue was put on top of an optical detector at different time points (0, 5 and 9 min), respectively.

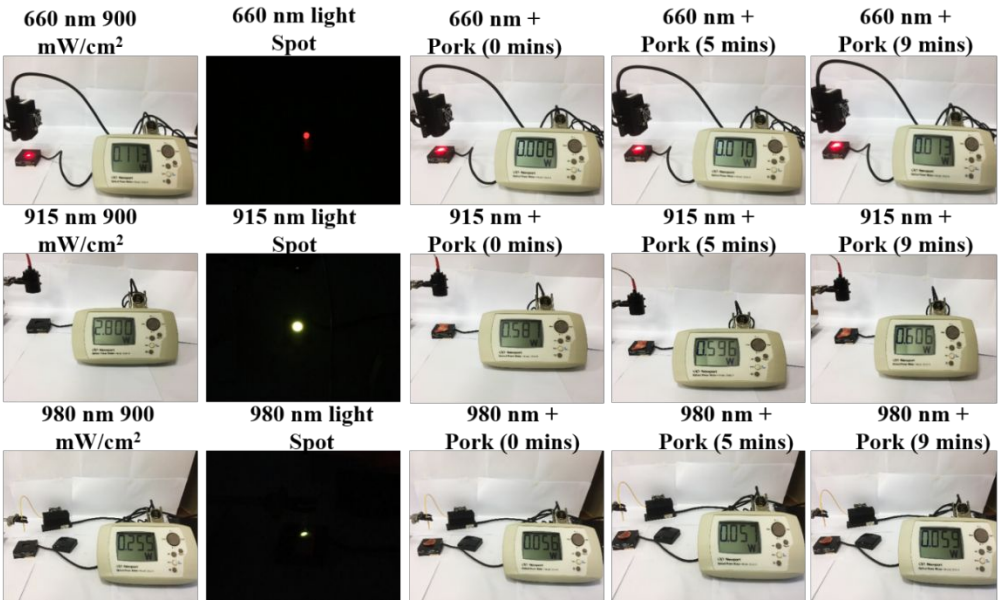

Figure S22. Optical images showing the experimental setup of light penetration though a pork tissue of 0.5 cm thickness for different laser wavelengths (660, 915 and 980 nm; all have the same laser power intensities of 900 mW/cm^2). The pork tissue was put on top of an optical detector at different time points (0, 5 and 9 min), respectively.

Table S1. Recent literature on NIR fluorescence imaging by using various fluorophores and NPs.

S.No	Material	Absorbance / emission	*In vitro /in vivo*	Application	Ref.
1	Au NEs	700–1700 nm/1160 nm	both	Tumor targeting imaging	S4
2	NIR712 doped NPs	660 nm/710 nm	both	Tumor targeting imaging	S5
3	BTPEPBI-NP50	543 nm/664 nm	both	Tumor targeting imaging	S6
4	NdF_3/SiO_2 core/shell NPs	730 nm/1056 nm	both	Tumor targeting imaging	S7
5	Dextran based ICG NPs	780 nm/805 nm	*in vitro*	cells	S8
6	Fe_3O_4/MnO NPs	675 nm/700 nm	*in vitro*	cells	S9
7	Nd:SrF_2 NPs	720 – 870 nm/1340 nm	both	Tumor targeting imaging	S10
8	Single-walled carbon nanotubes (SWNTs)	700-1100 nm	*in vitro*	Tumor targeting imaging	S11

Table S2. Brief literature review for nanomaterials-mediated phototherapies in comparison to the CuO/Cu_2O TNCs.

Nanomaterial	**Laser wavelength**	**Light Penetration (%)**	**Size (nm)**	**Absorption**	**Molar extinction coefficient ($M^{-1}cm^{-1}$)**	**η (%)**	**Ref.**
SWCNTs	808 nm	NR	r=0.6 L=150	700-1100 nm	7.9×10^6	NR	S11
$Cu_{7.2}S_4$ nanocrystals	980 nm	NR	20	950 nm	NR	57	S12
AuNR/GO nano hybrid	808 nm	NR	40	774 nm	NR	72	S13
Au nanoshells	808 nm	NR	110	Broad NIR	2×10^{10}	NR	S14
Bi_2S_3 nanoflowers	808 nm	NR	300	820 nm	NR	64	S15
Au nanorods	808 nm	NR	L=37 D=11	810 nm	1.02×10^9	NR	S16
$Ti_x Ta_{1-x} S_y O_z$	808 nm	NR	200-2000	620 nm	NR	39	S17
Au nanoshells	808 nm	NR	80	800-1100 nm	10^9	NR	S18
SPN_{1-11}	808 nm 1064 nm	NR	56	720 nm 1100 nm	NR	45 43	S19
$Cu_{2-x}Se$	808 nm	NR	16	970 nm	7.7×10^7	22	S20
Au NEs	915 nm 1064 nm	NR	350 ± 50	Broad NIR absorption	0.69×10^{12} 0.74×10^{12}	NR	S21
CuO/Cu_2O	660 nm 808 nm 915 nm 980 nm 1064 nm 1550 nm	11.5 20 21.6 23.1 24.6 33.4	280	600-1800 nm	0.83×10^{12} 0.90×10^{12} 0.94×10^{12} 0.95×10^{12} 0.95×10^{12} 0.89×10^{12}	73 67 78	Current work

**NR: Not Reported*

References

[S1] Y. Zhong, Z. Ma, S. Zhu, J. Yue, M. Zhang, A. L. Antaris, J. Yuan, R. Cui, H. Wan, Y. Zhou, W. Wang, N. F. Huang, J. Luo, Z. Hu, H. Dai, Boosting the Down-Shifting Luminescence of Rare-Earth Nanocrystals for Biological Imaging beyond 1500 nm. *Nat. Commun.* **2017**, 8, 737.

[S2] X. Liu, B. Li, F. Fu, K. Xu, R. Zou, Q. Wang, B. Zhang, Z. Chen, J. Hu, Facile Synthesis of Biocompatible Cysteine-Coated CuS Nanoparticles with High Photothermal Conversion Efficiency for Cancer Therapy**.** *Dalton Trans* **2014**, 43, 11709.

[S3] K. Rurack, M. Spieles, Fluorescence Quantum Yields of a Series of Red and Near-Infrared Dyes Emitting at 600−1000 nm. *Anal Chem* **2011**, 83, 1232-1242.

[S4] P. Vijayaraghavan, C.-S. Chiang, H. K. Chiang, M.-L. Li, K. C. Hwang, Multi-Branched Plasmonic Gold Nanoechinus-Based Triple Modal Bioimaging: An Efficient NIR-to-NIR Up and Down-Conversion Emission and Photoacoustic Imaging. *Adv. Matr. Technol.* **2016**, 1, 1600107.

[S5] J. Yu, X. Zhang, X. Hao, X. Zhang, M. Zhou, C.-S. Lee, X. Chen, Near-Infrared Fluorescence Imaging Using Organic Dye Nanoparticles. *Biomaterials* **2014**, 35, 3356.

[S6] Q. Zhao, K. Li, S. Chen, A. Qin, D. Ding, S. Zhang, Y. Liu, B. Liu, J. Z. Sun, B. Z. Tang, Aggregation-Induced Red-NIR Emission Organic as Effective and Photostable for Bioimaging**.** *J. Mater. Chem.* **2012**, 22, 15128-15135.

[S7] X.-F. Yu, L.-D. Chen, M. Li, M.-Y. Xie, L. Zhou, Y. Li, Q.-Q. Wang, Highly Efficient Fluorescence of NdF_3/SiO_2 Core/Shell Nanoparticles and the Applications for *in Vivo* NIR Detection. *Adv. Mater.* **2008**, 20, 4118.

[S8] P. Liu, C. Yue, B. Shi, G. Gao, M. Li, B. Wang, Y. Ma, L. Cai, Dextran Based Sensitive Theranostic Nanoparticles for Near-Infrared Imaging and Photothermal Therapy *in Vitro*. *Chem Commun (Camb)* **2013**, 49, 6143.

[S9] S. Li, C. Shao, W. Gu, R. Wang, J. Zhang, J. Lai, H. Li, L. Ye, Targeted Imaging of Brain Gliomas Using Multifunctional Fe_3O_4/MnO Nanoparticles. *RSC Advances* **2015**, 5, 33639.

[S10] I. Villa, A. Vedda, I. X. Cantarelli, M. Pedroni, F. Piccinelli, M. Bettinelli, A. Speghini, M. Quintanilla, F. Vetrone, U. Rocha, C. Jacinto, E. Carrasco, F. S. Rodríguez, Á. Juarranz, B. del Rosal, D. H. Ortgies, P. H. Gonzalez, J. G. Solé, D. J. García, 1.3 μm Emitting $SrF_2:Nd^{3+}$ Nanoparticles for High Contrast *in Vivo* Imaging in the Second Biological Window. *Nano Res.* **2014**, 8, 649.

[S11] N. W. S. Kam, M. O'Connell, J. A. Wisdom, H. Dai, Carbon Nanotubes as Multifunctional Biological Transporters and Near-Infrared Agents for Selective Cancer Cell Destruction. *Proc. Natnl. Acad. Sci.* **2005**, 102, 11600.

[S12] B. Li, Q. Wang, R. Zou, X. Liu, K. Xu, W. Li, J. Hu, $Cu_{7.2}S_4$ Nanocrystals: A Novel Photothermal Agent with a 56.7% Photothermal Conversion Efficiency for Photothermal Therapy of Cancer Cells. *Nanoscale* **2014**, 6, 3274.